1

REVISION 1

- Johnkoivulaite, Cs(Be₂B)Mg₂Si₆O₁₈, a new mineral of the beryl group from the gem deposits of Mogok,
 Myanmar
- 4 Aaron C. Palke^{1*}, Lawrence M. Henling², Chi Ma³, George R. Rossman³, Ziyin Sun¹, Nathan Renfro¹,
- 5 Anthony R. Kampf⁴, Kyaw Thu⁵, Nay Myo⁶, Patcharee Wongrawang⁷, Vararut Weeramonkhonlert⁷
- 6
- 7 ¹Gemological Institute of America, Carlsbad, CA 92008, USA
- 8 ²Beckman Institute, California Institute of Technology, Pasadena, CA 91125, USA
- ³Division of Geological and Planetary Sciences, California Institute of Technology, Pasadena, CA 91125,
- 10 USA
- ⁴Mineral Sciences Department, Natural History Museum of Los Angeles County, Los Angeles, California
 90007, USA
- 13 ⁵S Gemmological Institute, Yangon 11201, Myanmar
- 14 ⁶Greatland Gems and Jewelry, Mogok 11101, Myanmar
- ¹⁵ ⁷Gemological Institute of America, Bangkok 10500, Thailand
- 16 *E-mail: <u>apalke@gia.edu</u>
- 17
- 18

Abstract

- A new mineral of the beryl group, johnkoivulaite, Cs(Be₂B)Mg₂Si₆O₁₈, was recovered from the gem
- 20 gravels of the Pein Pyit area of the Mogok region in Myanmar. Thus far, only a single crystal has been
- 21 identified. It has dimensions about 5.8×5.7×5.5 mm. This specimen has an irregular shape but still has
- discernible crystal form with geometric growth patterns observed on the crystal faces. The crystal of
- 23 Johnkoivulaite is grayish-violet in color and strongly pleochroic going from nearly colorless with $E \perp c$ to
- 24 dark bluish-violet with E||c. Johnkoivulaite has a Mohs hardness of about 7½ and a measured density of
- 25 3.01(10) g cm⁻³. It is uniaxial (–) with ω = 1.607(1) and ε = 1.605(1) (white light). Electron microprobe
- 26 analyses gave the empirical formula of $(Cs_{0.85}K_{0.10}Na_{0.01})(Be_{1.88}B_{1.12})(Mg_{1.66}Fe_{0.27}Mn_{0.01}Al_{0.05})(Si_{5.98})O_{18}$ with
- 27 Be calculated by stoichiometry and confirmed by LA-ICP-MS measurements. Johnkoivulaite is hexagonal,
- 28 *P6/mmc* (#192) with *a* = 9.469(2), *c* = 9.033(2) Å, V = 701.5(3) Å³, and Z = 2. Johnkoivulaite is
- 29 isostructural with beryl and exhibits partial substitution of B for Be at the distorted tetrahedral site, Mg
- 30 for Al at the octahedral site, and Cs in the channel sites within the stacked Si_6O_{18} rings. This substitution
- 31 could be written as $(CsMg_2B)(\Box Al_2Be)_1$. Johnkoivulaite, the 7th member of the beryl group, is named in
- 32 honor of gemologist John Koivula in recognition of his contributions to mineralogy and gemology.
- 33 Keywords: beryl group, new mineral, gemology, johnkoivulaite, Mogok, Myanmar
- 34
- 35

Introduction

36 Mogok, Myanmar is one of the most gemologically diverse locales in the world. Not only does

- 37 Mogok produce some of the finest quality rubies, but it is also the source of some of the finest blue
- 38 sapphire, spinel, peridot, gem feldspar, and numerous other gems. The geological processes that
- 39 created the gemstone deposits in Mogok also created an assortment of rare minerals found nowhere
- 40 else in the world, such as painite and kyawthuite. Additionally, approximately 50 km NE of Mogok, near
- 41 the Momeik township, another rare mineral, avdeevite, of the beryl group was recently found, further
- adding to the geological diversity of this region. Another rare member of the beryl family, pezzottaite,
 has also been found in this region as well, being found in the Molo quarter of the Momeik township and
- 44 east of Let Pan Hla, Pyin Gyi Taung between the cities of Mandalay and Mogok.

45 In this contribution, we describe another rare mineral unique to Mogok, johnkoivulaite, also a 46 member of the beryl group. The new mineral was named in recognition of the lifetime work of John Koivula of the Gemological Institute of America and his many achievements and contributions to the 47 48 fields of mineralogy and gemology. The new mineral and name were approved by the IMA Commission 49 on New Minerals, Nomenclature, and Classification on September 6, 2019 under the number 2019-046. 50 The holotype specimen of johnkoivulaite is permanently deposited in the collection of the Gemological 51 Institute of America Museum under its catalogue number 41653 and the cotype consisting of several 52 tiny fragments from the holotype is deposited in the collections of the Natural History Museum of Los Angeles County, 900 Exposition Blvd., Los Angeles, California, USA, under catalogue number 75133. 53

54

Location and Geological Background

55 The Mogok gem deposits are found within the Mogok metamorphic belt stretching 56 approximately N-S from southern Myanmar in the Andaman Sea up into northern Myanmar near the 57 eastern Himalayan syntaxis (Searle et al. 2007). The Mogok metamorphic belt was produced by 58 compressive and transtensional deformation during the Himalayan orogeny in the late Cretaceous to the 59 Cenozoic time. The rubies and spinels in the Mogok region are hosted in relatively pure marbles 60 produced by this metamorphic event whereas blue sapphires and many of the other gems are more closely associated with igneous activity in the area, especially syenitic pegmatites that are often found 61 62 near the contacts between gneisses or marbles with large bodies of syenites or other alkaline intrusives 63 (e.g. Thu 2007). There is also a famous peridot mine near the north of the Mogok region related to hydrothermal alteration of an ophiolitic body emplaced during the Himalayan orogeny. Unfortunately 64 for the geologists interested in the finer details of the geological genesis of gem deposits, most of the 65 66 important gem mines in the Mogok region are secondary deposits except for some of the marble-hosted 67 ruby/spinel mines. In these secondary deposits, the precious gems have weathered out of their original 68 host rock and are washed downstream or downslope. As gem corundum and many other gem materials 69 are quite dense, they can get sequestered in gravel deposits in these secondary deposits.

70 This is also the case for the new mineral which was produced from an alluvial mining operation 71 in the Pein Pyit area (GPS coordinates: 22°58'33.92"N, 96°33'41.75"E) of the Mogok region of Myanmar. 72 Pein Pyit is a historic mining site in the Mogok region with most mining taking place in secondary alluvial 73 deposits. Ruby and spinel are the primary targets of mining activity, but sapphires, tourmaline, topaz, 74 and gem feldspar are also produced in the Pein Pyit area. The new mineral is a relatively hard and 75 refractory material that weathered out of the metamorphic and/or igneous rocks in the Pein Pyit area 76 and survived to be interred in a secondary alluvial deposit. It is unclear what the original host rock would 77 have been, but the dominant geological formations in the immediate area are marbles which are

intruded by granites and syenites with associated pegmatites of similar composition. The single sample
of the new mineral studied here was recovered as a single crystal and there is little direct evidence of
coexisting mineral assemblages. However, notable gem minerals also found in the Pein Pyit gem gravels
include danburite, poudretteite, hackmanite, orthoclase, scapolite, apatite, and muscovite which
indicate the importance of pegmatites in this area.

The stone was originally obtained by Nay Myo, a local gem dealer. Nay Myo recognized that the stone's basic properties didn't match any of the typical gem species expected from this area. He suspected this might be something new and so he submitted the stone to the Identification Laboratory of the Gemological Institute of America first in Bangkok, Thailand and then again in Carlsbad, California, USA.

88

Materials and Methods

89 LA-ICP-MS Chemical analyses

90 Laser Ablation Inductively-Coupled Plasma Mass Spectrometry (LA-ICP-MS) was used at the 91 Gemological Institute of America in Carlsbad, CA for chemical analysis of the new mineral using a 92 Thermo Fisher iCAP Qc ICP-MS, coupled with an Elemental Scientific NWR 213 laser ablation unit with a 93 frequency-quintupled Nd:YAG laser (213 nm wavelength) running at 4 ns pulse width. Ablation was 94 achieved using a 55 µm diameter laser spot size, a fluence (energy density) of approximately 10–12 J/cm², and a 20 Hz repetition rate. Argon was used as nebulizer gas (0.73 L/min), auxiliary gas (0.8 95 96 L/min), and cooling gas (14 L/min). Helium was used as the carrier gas at a flow rate of 0.8 L/min. Argon 97 and helium gas flow, torch position, sampling depth, and lens voltage were optimized to achieve maximum sensitivity (counts per concentration) and low oxide production rates (232 Th 16 O/ 232 Th <1%). 98 Ablated material was vaporized, atomized, and ionized by an argon plasma using a power of 1550 W. 99 The dwell time of each isotope measured was 0.01 second except ²⁸Si, which was measured for 0.005 100 second. The gas background was measured for 20 seconds, while the dwell time of each laser spot was 101 40 seconds. ²⁹Si was used as an internal standard with its initial value guessed with subsequent 102 103 renormalization of the results to produce 100 wt% oxides. GSD-1G, GSE-1G (U.S. Geological Survey), and NIST 610 were used as external standards. Isotopes measured for the elements reported here include 104 ⁹Be, ¹¹B, ²³Na, ²⁴Mg, ²⁷Al, ²⁹Si ³⁹K, ⁵⁵Mn, ⁵⁷Fe, and ¹³³Cs. Other isotopes including ⁷Li were measured as 105 well but were found at low concentrations (<1000 ppm) that would not affect the reporting of major 106 107 elements contributing to the stoichiometry of this mineral.

108 Electron Probe Microanalysis (EPMA)

109 Accurate chemical analyses were obtained at the California Institute of Technology on a JEOL 110 JXA-8200 electron microprobe. For all measured elements except B, 16 measurements were made using 111 analytical conditions of 15 kV accelerating voltage, 25 nA beam current, and a defocused beam diameter 112 of 10 µm. Separate B measurements were made with EPMA with 9 independent measurements using lower accelerating voltage of 10 kV, 30 nA, and a defocused beam diameter of 10 µm. Standards 113 employed were danburite (B), albite (Na), synthetic forsterite (Mg), anorthite (Al, Si), microcline (K), 114 synthetic tephroite (Mn), fayalite (Fe), and pollucite (Cs). [The danburite and pollucite standards were 115 116 developed specifically for this project. The danburite was essentially the pure endmember and the B_2O_3 concentration was determined by accurately measuring the CaO and SiO₂ concentrations and assuming 117 118 a stoichiometric formula with B₂O₃ making up the difference between 100 wt% and the sum of the CaO

- and SiO₂ wt%. The Cs₂O value for the pollucite standard was determined in a similar way by accurately
- measuring K₂O, Na₂O, Al₂O₃, and SiO₂ wt.% values, and ensuring charge balance and a stoichiometric
- 121 pollucite formula by forcing atoms of Al to equal the sum of K+Na+Cs. The total of the pollucite standard
- 122 came out at 99.3 wt.%.] Raw X-ray intensities were corrected for matrix effects with the CITZAF
- 123 procedure (Armstrong, 1995). Analytical precision is estimated to be ±1% relative for the major
- 124 elements and ±5% for the minor elements.

125 Raman Spectroscopy

126 Raman spectra were obtained using a Renishaw inVia Raman microscope system with a Modu-127 Laser Stellar-REN Ar-ion laser producing highly polarized light at 514 nm and collected at a nominal 128 resolution of 3 cm⁻¹ in the 2000–200 cm⁻¹ range. A 5x objective lens was used to focus the laser on the 129 surface of the sample.

130 Infrared Spectroscopy

Fourier-transform infrared (FTIR) spectroscopy was performed using a Thermo Nicolet 6700 FTIR spectrometer equipped with an XT-KBr beam splitter and a mercury-cadmium-telluride (MCT) detector operating with a 4x beam condenser accessory. The resolution was set at 2 cm⁻¹ with 1.928 cm⁻¹ data spacing. The spectrum was averaged from 200 acquisitions.

135 UV-Vis Spectroscopy

136 UV-Vis spectra were recorded with a PerkinElmer Lambda 950 in the range of 190–1100 nm with 137 a 1 nm spectral resolution and a scan speed of 400 nm/min.

138 Single Crystal X-Ray Diffraction

A small fragment broken off the main crystal was mounted on a polyimide MiTeGen loop with 139 140 STP Oil Treatment and placed in the 100 K nitrogen stream of an Oxford Cryosystems 700 Series Cryostream Cooler. X-ray data were collected with a Bruker AXS D8 KAPPA APEX II diffractometer 141 (Siemens KFF Mo 2K-90 fine-focus sealed tube with Mo K_{α} = 0.71073 Å operated at 50 kV and 30 mA; 142 143 TRIUMPH graphite monochromator; PHOTON 100 CMOS area detector with a resolution of 10.24 144 pixels/mm). A combination of 1526 ω - and ϕ -scans spanning 5° to 89° in 20 were collected with a 1° 145 width and collection times ranging from 5 to 25 seconds. All diffractometer manipulations including data 146 collection, integration, and scaling were carried out using the Bruker APEX3 software (Bruker, 2012). A 147 face-indexed absorption correction with μ refined was followed by a multiscan correction with an 148 additional spherical absorption correction with μ *r = 1.0 using SADABS (Bruker, 2001). The space group 149 was determined and the structure solved by intrinsic phasing using XT. Refinement was full-matrix least 150 squares on F^2 using XL. All atoms were refined using anisotropic displacement parameters. Full 151 crystallographic data are included in the Crystallographic Information Framework file (.cif), available as a supplementary file¹. 152

153 **Powder X-Ray Diffraction**

154 Powder X-ray studies were done using a Rigaku R-Axis Rapid II curved imaging plate 155 microdiffractometer, with monochromatized Mo*K* α radiation (λ = 0.71075 Å). A Gandolfi–like motion on 156 the ϕ and ω axes was used to randomize the samples and observed *d*-values and intensities were derived by profile fitting using JADE Pro software (Materials Data, Inc.). The cell parameters wererefined from the powder data using JADE Pro with whole pattern fitting.

159

Results

160 Physical and optical properties of johnkoivulaite

161 The single crystal of johnkoivulaite studied here occurs as an irregularly shaped crystal with 162 dimensions of 5.8×5.7×5.5 mm and weighing 0.234 g (**Figure 1**). Despite the lack of any well-defined 163 crystal form, the specimen has not been abraded by alluvial transport but appears to have discernible 164 crystal faces with geometric growth patterns observed on the surfaces. In fact, there does seem to be a 165 somewhat prismatic appearance to the crystal with what appears to be a basal pinacoid terminating one 166 end. However, whatever crystal form was present initially seems to be obfuscated by later etching along 167 the surfaces (**Figure 2**) and fracturing and breakage along one side.

168 Johnkoivulaite has a hardness of about 7½, a white streak, vitreous luster, and breaks in a brittle 169 fashion. There is no observable cleavage or parting and the stone exhibits conchoidal fracture. The density is 3.01(10) g cm⁻³ measured by weighing in air and again suspended in water. Note, the 170 estimated error is given by variations in measured density by repeat measurements. Additionally, the 171 172 density here is likely measured too low given the irregular shape of the crystal and the possibility that 173 small gas bubbles were trapped in small cracks and cavities on the stone's surface, despite the authors' 174 best efforts to remove such features during measurement. The stone is non-fluorescent in longwave 175 (~360 nm) or shortwave (~254 nm) standard UV lamps. Johnkoivulaite has a uniaxial optic character as 176 determined by observation of its optic figure in a gemological polariscope. A small chip was removed 177 from the sample and a uniaxial negative interference figure was observed on a petrographic microscope. 178 The indices of refraction were determined to be $\omega = 1.607(1)$ and $\varepsilon = 1.605(1)$ using standard refractive 179 index liquids.

180 The holotype crystal of johnkoivulaite is slightly grayish violet when viewed in daylight. Of 181 particular note is the stone's extreme pleochroism going from nearly colorless (with the polarized 182 electric vector of the light $E\perp c$, or as the o-ray) to dark bluish-violet (with the polarized electric vector 183 $E\parallel c$, or as the e-ray) when observed in polarized light (**Figure 3**). However, no pleochroism was 184 observable in the small crystal fragments used for the optical measurements.

Observations of the stone's inclusions unfortunately did not shed light on the geological origin of the mineral. The only internal features that could be discerned were linear tubes that appear to be crystallographically aligned with the c-axis, which seem to have been infiltrated by fluids which precipitated what are likely to be iron-oxide minerals. These tubes are interpreted to be either growth tubes or etch tubes (**Figure 4**), which are common inclusions in beryl and other pegmatite minerals (Gubelin and Koivula 1986).

191

192

193 Raman spectroscopic data

194 When the new mineral was first submitted to the Identification lab at the Gemological Institute 195 of America, its measured properties did not match any obvious known mineral species. Therefore, the

5

196 first additional piece of evidence sought was Raman spectroscopy that can be a very powerful

- 197 fingerprinting tool for mineral species when a robust reference database is available. The Raman
- spectrum of johnkoivulaite is shown in **Figure 5**. When referenced against the RRUFF database there
- were no complete matches. The closest match, however, was with beryl. The dominant peaks in the
 Raman spectrum of johnkoivulaite occur at 1084 cm⁻¹, 691 cm⁻¹, 623 cm⁻¹, 405 cm⁻¹, 260 cm⁻¹, and 226
- Raman spectrum of johnkoivulaite occur at 1084 cm⁻¹, 691 cm⁻¹, 623 cm⁻¹, 405 cm⁻¹, 260 cm⁻¹, and 226
 cm⁻¹, which generally matche with the dominant bands in beryl at 1067 cm⁻¹, 683 cm⁻¹, 396 cm⁻¹, and 323
- 202 cm⁻¹ (from the RRUFF database, Lafuente et al. 2015). **Figure 5** shows the polarized Raman spectra the
- polarized component of the light E || c and $E \perp c$. For endmember beryl, there are a large number of peaks
- in the range of 100-1500 cm⁻¹ which previous workers have attributed to vibrations of the Si₆O₁₈ rings,
- with or without involvement of neighboring BeO_4 and/or AlO₆ groups (Adams et al. 1974; Hagemann et
- al. 1990; Kim et al. 1995). The overall similarity between the Raman spectrum of johnkoivulaite and that
- of beryl suggests the Raman bands observed between 1100 and 100 cm⁻¹ for johnkoivulaite are related
- to vibrational modes of the Si₆O₁₈ rings potentially with the involvement of MgO₆ and BeO₄ or BO₄
 groups. However, the more complex composition of johnkoivulaite precludes a deeper comparison and
- 210 assignment of individual vibrational bands.
- 211

212 IR spectroscopic data

The FTIR spectrum of johnkoivulaite shows two strong absorption bands at 3589 cm⁻¹ and 3659 cm⁻¹ (Figure 6). These peaks correspond to molecular water in the channels of the crystal structure. Given the high alkali content of johnkoivulaite and comparison with IR spectra of alkali-rich beryl, these peaks are likely equivalent to the type II water species seen in the IR spectra of alkali-rich beryl in which the water is associated with alkali ions contained in the channels (Aurisicchio et al. 1994).

218

219 UV-Visible absorption spectroscopic data

220 The main absorption feature seen in the UV-Vis absorption spectrum is the broad band around 560 nm (Figure 7). With the polarized component of the light E||c (or measuring the e-ray), this feature 221 222 absorbs a significant portion of the green, yellow, and orange light passing through the stone while 223 allowing much of the red and blue light to pass through, imparting a deep violet color with E||c 224 polarized light (the e-ray). On the other hand, this feature nearly disappears with the polarized component of the light $E \perp c$ (or measuring the o-ray absorption) and there is very little absorption of 225 226 visible light . Another absorption feature observed is the band at about 850 nm in the near-IR which 227 does not change much with polarization of the light and does not significantly affect the color of this 228 material. This absorption spectrum is similar to that seen for aquamarine (blue beryl) only the 229 polarizable broad band around 560 nm is shifted down in energy in beryl to about 680 nm and most of the red light gets absorbed leading to a purer blue color. Aquamarine is also significantly pleochroic 230 going from blue to nearly colorless due to this similar absorption feature (e.g. Palke and Hapeman 231 2019). This absorption feature in aquamarine is caused by Fe²⁺-Fe³⁺ intervalence charge transfer (IVCT) 232 (Fritsch and Rossman 1988). This Fe²⁺-Fe³⁺ IVCT is likely the cause of the absorption band at 560 nm in 233 johnkoivulaite. Note, a similar feature is seen as well in cordierite and is also attributed to Fe²⁺-Fe³⁺ IVCT 234 (Taran and Rossman 2001). Another possible explanation of this band at 560 nm in johnkoivulaite is the 235 possible presence of Mn³⁺ as in red beryl. However, the polarization of Mn³⁺ behavior in beryl is not 236

- consistent with the polarization of the 560 nm band in johnkoivulaite (e.g. Nassau and Wood 1968;
- Fridrichová et al. 2018). Aquamarine also shows a similar near-IR, absorption band around 830 nm that
- has been ascribed to octahedrally-coordinated Fe²⁺ (Taran and Rossman 2001), which suggests the 850
- nm band in johnkoivulaite has a similar origin. The relatively narrow and weak absorption bands
- sometimes seen in aquamarine at around 370 nm and 430 nm related to octahedral Fe³⁺ are not
- 242 observed in johnkoivulaite.
- 243

244 Chemical composition

The chemical composition of johnkoivulaite was first investigated using LA-ICP-MS. While not generally considered to be as quantitatively accurate as EPMA for major elements, LA-ICP-MS has the advantage of being able to measure most of the periodic table in a single analysis as well as having much greater sensitivity than EPMA, allowing trace elements to be readily detected. The major elements measured by LA-ICP-MS were Be, B, Mg, Si, Fe, and Cs. Additionally, Na, Al, K, and Mn were picked up as minor elements while only traces of other elements were measured (**Table 1**).

251 Using the preliminary chemical data from LA-ICP-MS, we were able to take a more focused 252 approach to the EPMA analysis. As discussed in the methods section, our EPMA analyses were able to 253 measure all of the major and minor elements in johnkoivulaite except for Be, even though wavelength 254 scans were employed in an attempt to make at least qualitative measurements of Be. Additionally, our B 255 measurements were taken during a different EPMA session on different spots than the rest of the major 256 and minor elements. The LA-ICP-MS analysis indicates that the only major element not detected by 257 EPMA was Be. Given the data collected so far which suggest the new mineral belongs to the beryl family, 258 we can impose the constraints that there must be 18 O per formula and we can assume that both Be 259 and B would occupy the distorted tetrahedral site in a beryl group structure and that the sum of Be and 260 B must equal 3. Using these constraints, the wt% BeO was calculated from this formula with the 261 resulting wt% oxide sums coming out to 101.53 wt%. The results of EPMA measurements are given in 262 Table 2. In general, the LA-ICP-MS analyses is in surprisingly good agreement with the EPMA 263 measurements. Based on the EPMA measurements, the full empirical chemical formula of johnkoivulaite 264 can be given as $(Cs_{0.85}K_{0.10}Na_{0.01})(Be_{1.88}B_{1.12})(Mg_{1.66}Fe_{0.27}Mn_{0.01}AI_{0.05})(Si_{5.98})O_{18}$ and the generalized ideal chemical formula is Cs(Be₂B)Mg₂Si₆O₁₈. 265

266

267 Crystal structure of johnkoivulaite

A small fragment (0.18 x 0.33 x 0.47 mm) removed from the holotype specimen was used for the single-crystal X-ray structure analysis. Johnkoivulaite (as well as beryl) crystallizes in the hexagonal space group *P6/mmc* (# 192), with *a* = 9.469(2) Å, *c* = 9.033(2) Å, V = 701.5(3) Å³, and Z = 2. The calculated density of johnkoivulaite is 3.117 g/cm³ using the empirical formula and 3.157 g/cm³ with the ideal formula, which are in reasonably good agreement with the measured density of 3.01(10) g/cm³.

The main structural units of johnkoivulaite are the Si_6O_{18} rings, which are stacked along the **c**axis creating large channels into which the Cs atoms are stuffed at the 2a position in a site coordinated by 12 O atoms. While this site is vacant in the pure beryl structure, this is where Cs and other large alkali 276 cations are located in alkali-rich beryl (Brown and Mills 1986; Aurisicchio et al. 1988). The Si₆O₁₈ rings are 277 interlinked by distorted (B,Be)O₄ tetrahedra and MgO₆ octahedra.

278 With the chemical analyses described above as a starting basis, the site occupancies can be 279 refined to give an empirical formula for this specimen of johnkoivulaite. Based on chemical analysis, the 280 Cs site was refined as a mixture of Cs and K (0.81:0.19, site constrained to full occupancy); the Mg site as 281 a mixture of Mg and Fe (1.72:0.29, site constrained to full occupancy); and the Be site as a mixture of Be 282 and B (2.08:0.93), site constrained to full occupancy). The Be to B ratio is more unreliable than the 283 statistics suggest due to the significant X-ray absorption by cesium compounded by the irregular shape 284 of the sample. The minor constituents Na, Mn, and Al were not included in the model.

285 The atomic coordinates and displacement parameters for johnkoivulaite are given in Tables 3-4 286 and selected bond distances are given in **Table 5**. The structure of johnkoivulaite is illustrated in **Figures** 287 8-9.

288 A few small chips (~100-400 μ m in size) were removed from the specimen of johnkoivulaite and 289 gently crushed for powder X-Ray diffraction. The powder XRD data was indexed using the structure 290 derived from single crystal XRD measurements and is reported in Table 6. Cell parameters refined from the powder XRD data are a = 9.4657(11), c = 9.0374(12) Å and V = 701.26(19) Å³ 291

292

293 Relationship to other members of the beryl group

294 Relative to beryl, in ideal endmember johnkoivulaite, one out of three Be atoms in the distorted 295 tetrahedral sites is replaced by B, all octahedral Al is replaced by Mg, Si occupies all the polymerized 296 tetrahedral sites in the ring structures, and a Cs atom sits within the channel sites at the 2a position. 297 One of the major differences between johnkoivulaite and beryl is the addition of a discrete structural site for Cs⁺ in johnkoivulaite. The addition of this cation in the channel is balanced by the substitution of 298 Mg^{2+} for Al^{3+} in the octahedral site, as well as by B^{3+} replacing Be^{2+} in one out of three distorted 299 tetrahedral sites. Technically, this can be written as the substitution (CsMg₂B)(\Box Al₂Be)₋₁. This is similar to 300 301 another member of the beryl group, pezzottaite [Cs(Be₂Li)Al₂Si₆O₁₈], which also has a discrete structural 302 site for Cs. The charge balanced substitution between johnkoivulaite and pezzottaite can be written as 303 $(Mg_2B)(Al_2Li)_{-1}$. The seven members of the beryl group are listed in **Table 7**.

304 Chemically, johnkoivulaite is similar to pezzottaite in which heterovalent substitutions occur for 305 Be in the distorted tetrahedral site. However, johnkoivulaite is structurally distinct from pezzottaite in 306 that both Be and B occupy the same structurally and symmetrically identical site in johnkoivulaite 307 whereas in pezzottaite this site is split, with Be and Li occupying structurally and symmetrically distinct 308 sites. For this reason, johnkoivulaite maintains the higher symmetry space group of P6/mcc while 309 pezzottaite has an ordered superstructure with lower symmetry trigonal space group of R3c. 310 Johnkoivulaite is structurally more similar to Cs-rich beryl (Lambruschi et al. 2014). 311

312

Implications

Johnkoivulaite's unusual crystal chemistry 313

The chemistry of johnkoivulaite is unusual from a geochemical perspective. Two of the elements 314 315 that occur as major elements in johnkoivulaite, Mg and Cs, are typically concentrated in distinct rock 316 types that are generally geologically unrelated. Cs is usually enriched in granitic and alkali-rich igneous 317 rocks as well as in their associated pegmatites. On the other hand, Mg is usually relatively poor in those 318 rocks but is enriched in rocks that are generally Cs-poor, such as (ultra)mafic/basic rocks and to an 319 extent in some marbles. However, this apparent geochemical contradiction might actually provide some 320 clues to the geological genesis story of the gem deposits in Mogok. The formation of rubies in the 321 marbles is understood to be related to the concentration and mobilization of Al and Cr from clay-rich 322 layers in the original limestones, potentially facilitated by the movement of molten salts within the 323 marbles, eventually leading to crystallization of Cr-rich corundum (Garnier et al. 2008). However, given 324 that most of the gem deposits are secondary and there is relatively little exposure of gem-bearing 325 primary host rocks, the specific geological conditions needed to form some of the other gemstones, 326 such as the sapphires, are less well understood. The current thinking by most researchers is that 327 sapphires formed in syenitic pegmatites through interaction with marbles or other metamorphic rocks 328 into which the pegmatites were injected (Thu 2007). The unusual chemistry of johnkoivulaite seems to 329 support the latter part of this hypothesis. This unique chemistry could have been formed by the 330 introduction of Cs from pegmatites which intruded into marbles or other metamorphic rocks that were

331 enriched in Mg.

332 Occupancy and hydration of the channel sites in johnkoivulaite

333 The nearly full occupancy of the 2a channel site is another unique aspect of the structure. The implication is that johnkoivulaite must be a relative dry (water-poor) member of the beryl group. The 2a 334 channel sites are separated from each other by a distance of 4.517 Å in johnkoivulaite. If all the 2a sites 335 are occupied by Cs^+ ions with ionic radii of 1.88 Å, there is a distance of only 0.757 Å between the Cs^+ 336 337 ions. This precludes the presence of an H_2O molecule in the 2b site, which is between adjacent 2a sites. Nonetheless, the FTIR spectra did indicate the presence of H_2O in johnkoivulaite. Given that the 338 339 occupation of the 2a site is only at 96% capacity, it is expected that there should be some limited room 340 for H₂O molecules in the 2b site.

On the other hand, most members of the beryl group have well below 50% occupancy of alkali cations at the 2a site allowing for significant occupation of the 2b site by H₂O molecules. One major exception to this is pezzottaite which often has >50% occupancy of the 2a site, but never approaches the 2a site occupancy of johnkoivulaite. In this regard, johnkoivulaite can be considered a stuffed, comparatively dry beryl group mineral.

346

347

Acknowledgments

We thank two peer reviewers for their constructive comments and suggestions that have strengthened this manuscript. We also thank Dr. Mike Breeding (GIA) and Dr. Evan Smith (GIA) for reading the manuscript and providing additional comments and editing for grammar and style. Much gratitude is owed to Associate Editor Fabrizio Nestola and the rest of the editorial staff at American Mineralogist as well. The Bruker D8 Kappa X-ray diffractometer was purchased via an NSF CRIF:MU award to the California Institute of Technology (CHE-0639094) and upgraded with a Dow Next Generation Instrumentation Grant. EPMA analysis was carried out at the Caltech GPS Division Analytical Facility, 355 which is supported, in part, by NSF Grants EAR-0318518 and DMR-0080065. George Rossman's 356 contribution to this work was also supported by NSF grant EAR-1322082. A portion of this study was 357 funded by the John Jago Trelawney Endowment to the Mineral Sciences Department of the Natural 358 History Museum of Los Angeles County. 359 360 **References Cited** 361 Adams, D.M., and Gardner, I.R. (1974) Single-crystal vibrational spectra of beryl and dioptase. Journal of 362 the Chemical Society, Dalton Transactions, 14, 1502-1505. 363 Armstrong, J.T. (1995) CITZAF: a package of correction programs for the quantitative electron 364 microbeam X-ray analysis of thick polished materials, thin films, and particles. Microbeam Analysis, 365 4, 177-200. 366 Aurisicchio, C., Fioravanti, G., Grubessi, O., and Zanazzi, P.F. (1988) Reappraisal of the crystal chemistry 367 of beryl. American Mineralogist, 73, 826-837. 368 Aurisicchio, C., Grubessi, O., and Zecchini, P. (1994) Infrared spectroscopy and structural chemistry of 369 the beryl group. The Canadian Mineralogist, 32, 55-68. 370 Brown, G.E. and Mills, B.A. (1986) High-temperature structure and crystal chemistry of hydrous alkali-371 rich beryl from the Harding pegmatite, Taos County, New Mexico. American Mineralogist, 71, 547-372 556. 373 Bruker (2001) SADABS. Bruker AXS Inc., Madison, Wisconsin, USA. 374 Bruker (2012) APEX3. Bruker AXS Inc., Madison, Wisconsin, USA. Fridrichová, J., Bačík, P., Ertl, A., Wildner, M., Dekan, J., and Miglierini, M. (2018) Jahn-Teller distortion of 375 Mn³⁺-occupied octahedral in red beryl from Utah indicated by optical spectroscopy. Journal of 376 377 Molecular Structure, 1152, 79-86. 378 Fritsch, E., and Rossman, G. R. (1988). An update on color in gems. Part 2: Colors involving multiple 379 atoms and color centers. Gems & Gemology, 24, 3-15. 380 Garnier, V., Giuliani, G., Ohnenstetter, D., Fallick, A.E., Dubessy, J., Banks, D., Vinh, H.Q., Lhomme, T., 381 Maluski, H., Pêcher, A. and Bakhsh, K.A. (2008). Marble-hosted ruby deposits from Central and 382 Southeast Asia: Towards a new genetic model. Ore Geology Reviews, 34, 169-191. Gübelin, E., & Koivula, J. I. (1986). Photoatlas of Inclusions in Gemstones (ABC, Zurich). 383 384 Hagemann, H., Lucken, A., Bill, H., Gysler-Sanz, J., and Stalder, H.A. (1990) Polarized Raman spectra of 385 beryl and bazzite. Physical Chemistry of Minerals, 17, 395-401. Kim, C.C., Bell, M.I., and McKeown, D.A. (1995) Vibrational analysis of beryl (Be3Al2Si6O18) and its 386 387 constituent ring (Si6O18). Physica B: Condensed Matter, 205, 193-208. Lafuente B, Downs R T, Yang H, Stone N (2015) The power of databases: the RRUFF project. In: Highlights 388 389 in Mineralogical Crystallography, T Armbruster and R M Danisi, eds. Berlin, Germany, W. De Gruyter, 390 pp 1-30

Lambruschi, E., Gatta, G.D., Adamao, I., Bersani, D., Salvioli-Mariani, E., Lottici, P.P. (2014) Raman and
 structural comparison between the new gemstone pezzottaite Cs(Be₂Li)Al₂Si₆O₁₈ and Cs-beryl.
 Journal of Raman Spectroscopy, 45, 993-999.

- Momma, K. and Izumi, F. (2011) VESTA 3 for three-dimensional visualization of crystal, volumetric and morphology data. Journal of Applied Crystallography, 44, 1272-1276.
- Nassau, K. and Wood, D.L. (1968) An examination of red beryl from Utah. American Mineralogist, 53,
 801-806.
- Palke, A.C., and Hapeman, J. (2019) New find of deep blue aquamarine from Nasarawa State in Nigeria,
 Gems & Gemology, 55, 437-439.
- Searle, M. P., Noble, S. R., Cottle, J. M., Waters, D. J., Mitchell, A. H. G., Hlaing, T., & Horstwood, M. S. A.
 (2007). Tectonic evolution of the Mogok metamorphic belt, Burma (Myanmar) constrained by U-ThPb dating of metamorphic and magmatic rocks. Tectonics, 26.
- Sheldrick, G.M. (2015a) SHELXT integrated space-group and crystal-structure determination. Acta
 Crystallographica, A71, 3–8.
- 405 Sheldrick, G.M. (2015b) Crystal structure refinement with SHELXL. Acta Crystallographica, C71, 3–8.
- Taran, M. N., and Rossman, G. R. (2001). Optical spectroscopic study of tuhualite and a re-examination
 of the beryl, cordierite, and osumilite spectra. American Mineralogist, 86(9), 973-980.
- Thu, K. (2007). The igneous rocks of the Mogok Stone Tract: their distribution, petrography,
 petrochemistry, sequence, geochronology and economic geology. Yangon University, Yangon.
- 410
- 411

Figure Captions

- 412 Figure 1: Photo of the single confirmed specimen of johnkoivulaite. Photo by Robert Weldon. ©GIA
- **Figure 2:** Photomicrograph of the surface of johnkoivulaite showing a slightly corroded pattern. Field of view 1.44 mm. Photomicrograph by Nathan Renfro. ©GIA
- Figure 3: Photomicrograph of johnkoivulaite with light polarized parallel to the e-ray (left) and o-ray
 (right). Fields of view 10.05 mm. ©GIA
- 417 **Figure 4:** Photomicrograph of the inclusions within johnkoivulaite which include growth tubes (or etch
- tubes) which are crystallographically aligned to the johnkoivulaite host. Field of view 4.12 mm.
- 419 Photomicrograph by Nathan Renfro. ©GIA
- 420 **Figure 5:** Raman spectra of johnkoivulaite in both E||c (blue) and $E\perp c$ (orange) polarization.
- 421 **Figure 6:** FTIR spectrum of johnkoivulaite
- 422 **Figure 7**: UV-Vis spectrum of johnkoivulaite compared against that of deep blue aquamarine (beryl)
- 423 from Nigeria (Palke and Hapeman 2019). Note, spectra are offset vertically for the sake of comparison.

- 424 **Figure 8:** A VESTA 3 (Momma and Izumi, 2011) structural diagram of johnkoivulaite down the *c*-axis. O
- 425 atoms are shown in red, SiO_4 tetrahedra in blue, MgO_6 octahedra in orange, BeO_4 tetrahedra in green, 426 and Cs atoms in light blue. The black line shows the unit cell.
- 427 **Figure 9:** A VESTA 3 (Momma and Izumi, 2011) structural diagram of johnkoivulaite almost
- 428 perpendicular to the *c*-axis showing the stacked Si_6O_{18} rings which define a channel in which the Cs
- 429 atoms reside. O atoms are shown in red, SiO_4 tetrahedra in blue, MgO_6 octahedra in orange, BeO_4
- 430 tetrahedra in green, and Cs atoms in light blue. The black line shows the unit cell.
- 431

432

- 433 Endnote:
- ¹Deposit item AM-20-XXXXX, CIF. Deposit items are free to all readers and found on the MSA website,
- 435 via the specific issue's Table of Contents (go to
- 436 http://www.minoscam.org/MSA/AmMin/TOC/2020/Xxx2020_data/Xxx2020_data.html).

Table 1. LA-ICP-MS results (in wt%) measuredfor johnkoivulaite averaged over 6 spotanalyses and renormalized to 100 wt% oxides.

Constituent	Mean
BeO	9.58
B ₂ O ₃	4.66
Na ₂ O	0.03
MgO	10.08
AI_2O_3	0.39
SiO ₂	54.19
K ₂ O	0.70
MnO	0.11
FeO	3.04
Cs ₂ O	17.20
Total	99.98

Constituent	Mean	Range SD		Standard
BeO*	7.25			
B_2O_3	5.99	5.79-6.29	0.14	danburite
Na ₂ O	0.04	0.01-0.08	0.02	albite
MgO	10.34	10.24-10.43	0.06	syn. forsterite
AI_2O_3	0.38	0.35-0.41	0.02	anorthite
SiO ₂	55.36	54.56-55.68	0.11	anorthite
K ₂ O	0.71	0.69-0.73	0.01	microcline
MnO	0.10	0.07-0.12	0.02	Syn. tephroite
FeO	2.98	2.92-3.04	0.04	fayalite
Cs ₂ O	18.36	18.15-18.79	0.14	pollucite
Total	101.51			
* calculated to satisfy beryl-type formula with 18 O and Be+B = 3.				

Table 2: Electron Microprobe Analytical data (in wt%) measured for johnkoivulaite.

Table 3: Atomic coordinates, equivalent isotropic displacement parameters					
(Å ²), an	(Å ²), and occupancies for johnkoivulaite.				
	x/a	y/b	z/c	U_{eq}	Occ.
Cs	0	0	0.25	0.01208(3)	0.814(2)
К	0	0	0.25	0.01208(3)	0.186(2)
Si	0.62438(2)	0.72095(2)	0.5	0.00426(4)	1
Mg	0.33333	0.66667	0.75	0.00514(9)	0.857(3)
Fe	0.33333	0.66667	0.75	0.00514(9)	0.143(3)
O(1)	0.51928(4)	0.64492(4)	0.64773(4)	0.00978(6)	1
O(2)	0.78438(6)	0.70106(6)	0.5	0.01045(7)	1
Ве	0.5	0.5	0.75	0.0049(3)	0.69(4)
В	0.5	0.5	0.75	0.0049(3)	0.31(4)

Table 2: Atomic coordinatos, oquivalent isotronic displace ont n .

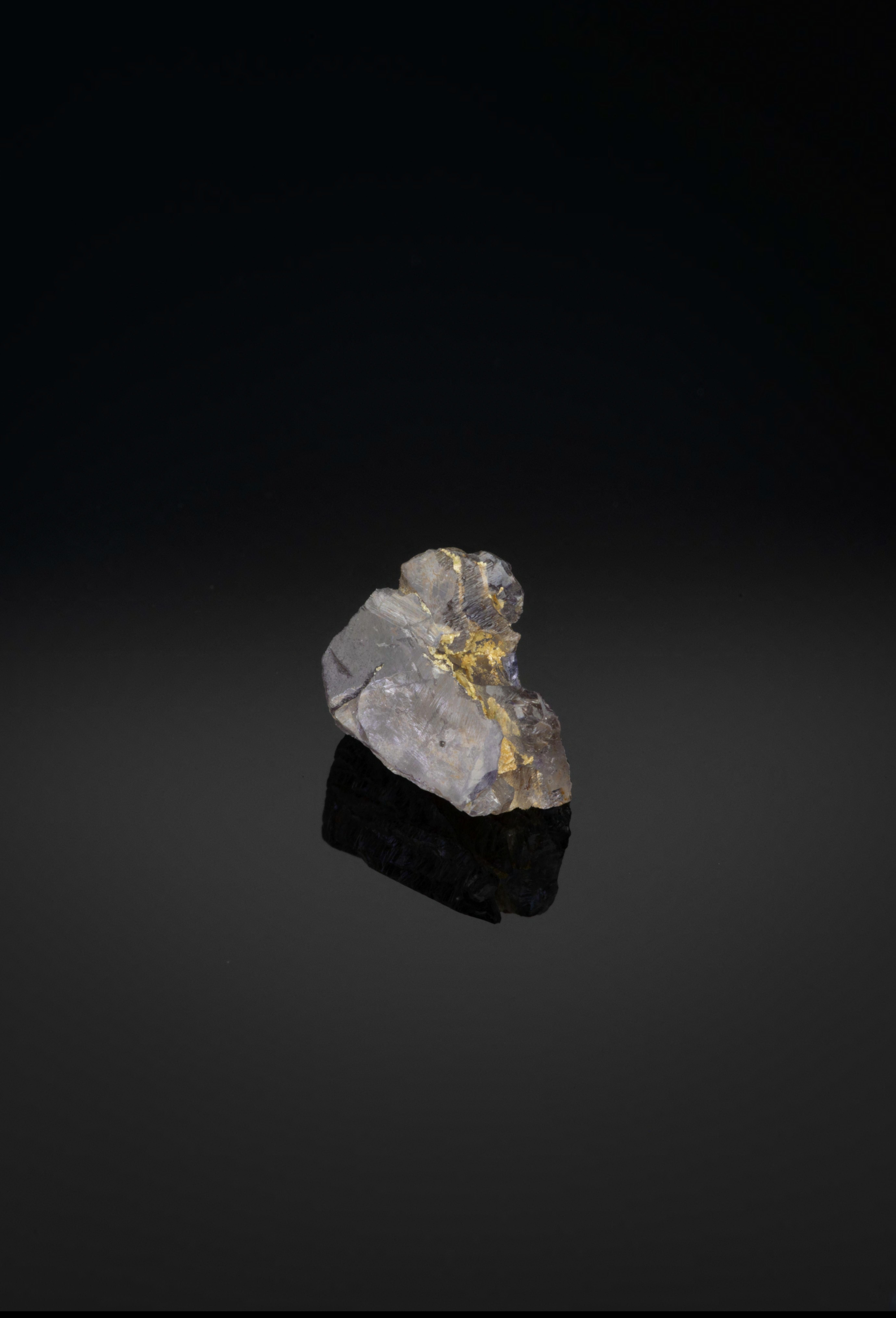
Table 4: Anisotropic displacement parameters (Å ²) for johnkoivulaite. The anisotropic						
displa	displacement factor exponent takes the form: $-2\pi^2$ [$h^2 a^{*2}U^{11} + + 2 h k a^* b^* U^{12}$]]
	U11	U22	U33	U23	U13	U12
Cs	0.01390(4)	0.01390(4)	0.00844(4)	0	0	0.00695(2)
К	0.01390(4)	0.01390(4)	0.00844(4)	0	0	0.00695(2)
Si	0.00363(6)	0.00359(6)	0.00535(6)	0	0	0.00166(4)
Mg	0.00534(10)	0.00534(10)	0.00475(13)	0	0	0.00267(5)
Fe	0.00534(10)	0.00534(10)	0.00475(13)	0	0	0.00267(5)
O(1)	0.00956(11)	0.00724(10)	0.01092(11)	0.00033(8)	0.00510(9)	0.00299(9)
O(2)	0.00612(14)	0.0087(2)	0.0188(2)	0	0	0.00535(12)
Be	0.0050(3)	0.0050(3)	0.0048(4)	0	0	0.0026(3)
В	0.0050(3)	0.0050(3)	0.0048(4)	0	0	0.0026(3)

Table 5: Selected bond				
distances (Å) for	distances (Å) for			
johnkoivulaite.				
Cs-O(2)	3.3915(6)			
Si-O(1)	1.6041(4)			
Si-O(2)	1.6176(6)			
Mg-O(1)	2.0878(5)			
Mg-Be	2.7336(6)			
O(1)-Be	1.5872(4)			

johnkoivulaite. Calculated lines with $I > 1.5$ are					
listed.					
I _{obs}	$d_{ m obs}$		$d_{ m calc}$	Icalc	hkl
13	8.197		8.2004	5	$1\ 0\ 0$
10	4.743		4.7345	4	110
17	4.106		4.1002	7	200
4	3.967		3.9562	2	102
100	3.272		3.2681	100	112
82	3.064	5	3.0995	19	210
62	5.004	l	3.0359	43	202
85	2.940		2.9317	40	211
22	2.737		2.7335	14	300
7	2.559		2.5556	4	212
18	2.359	5	2.3673	6	220
10	2.559	1	2.3385	5	302
27	2 274	5	2.2744	9	310
27	2.274	1	2.2583	8	004
22	2.185		2.1773	9	104
18	2.100		2.0967	9	222
0	2 0 2 0	5	2.0383	2	114
8	2.039	1	2.0314	2	312
10	1.8716		1.8668	5	402
7	1.8461		1.8418	3	321
17	1 0070	5	1.8252	4	214
17	1.8272	1	1.8148	5	313
29	1.7939		1.7895	16	410
		(1.7554	2	411
40	1.7444	3	1.7410	16	304
		L	1.7367	6	322
24	1.6665		1.6637	14	412
25	1.6390		1.6340	14	224
6	1.6016		1.6025	2	314
			1.5609	2	215
		(1.5497	4	420
30	1.5444	3	1.5416	3	502
		l	1.5383	7	413
18	1.4912	• 3	1.4898	7	332
			1.4728	2	510
13	1.4381		1.4348	9	116
		5	1.4133	2	206
7	1.4110	ì	1.4025	3	414
		- >			

Table 6. Powder diffraction data (d in Å) for

Table 7: Minerals of the beryl group			
		Symmetry (Space	
	Ideal Chemical Formula	Group)	
Beryl	$Be_3AI_2Si_6O_{18}$	P 6/mmc	
Bazzite	$Be_3Sc_2Si_6O_{18}$	P 6/mmc	
Indialite	(Mg ₂ Al)Al ₂ (AlSi ₅)O ₁₈	P 6/mmc	
Ferroindialite	$[(Fe^{2+},Mg)_2AI]AI_2(AISi_5)O_{18}$	P 6/mmc	
Stoppaniite	$Be_3Fe_{2}^{3+}Si_6O_{18}\cdot H_2O$	P 6/mmc	
Johnkoivulaite	Cs(Be ₂ B)Mg ₂ Si ₆ O ₁₈	P 6/mmc	
Pezzottaite	Cs(LiBe ₂)Al ₂ Si ₆ O ₁₈	R 3c	









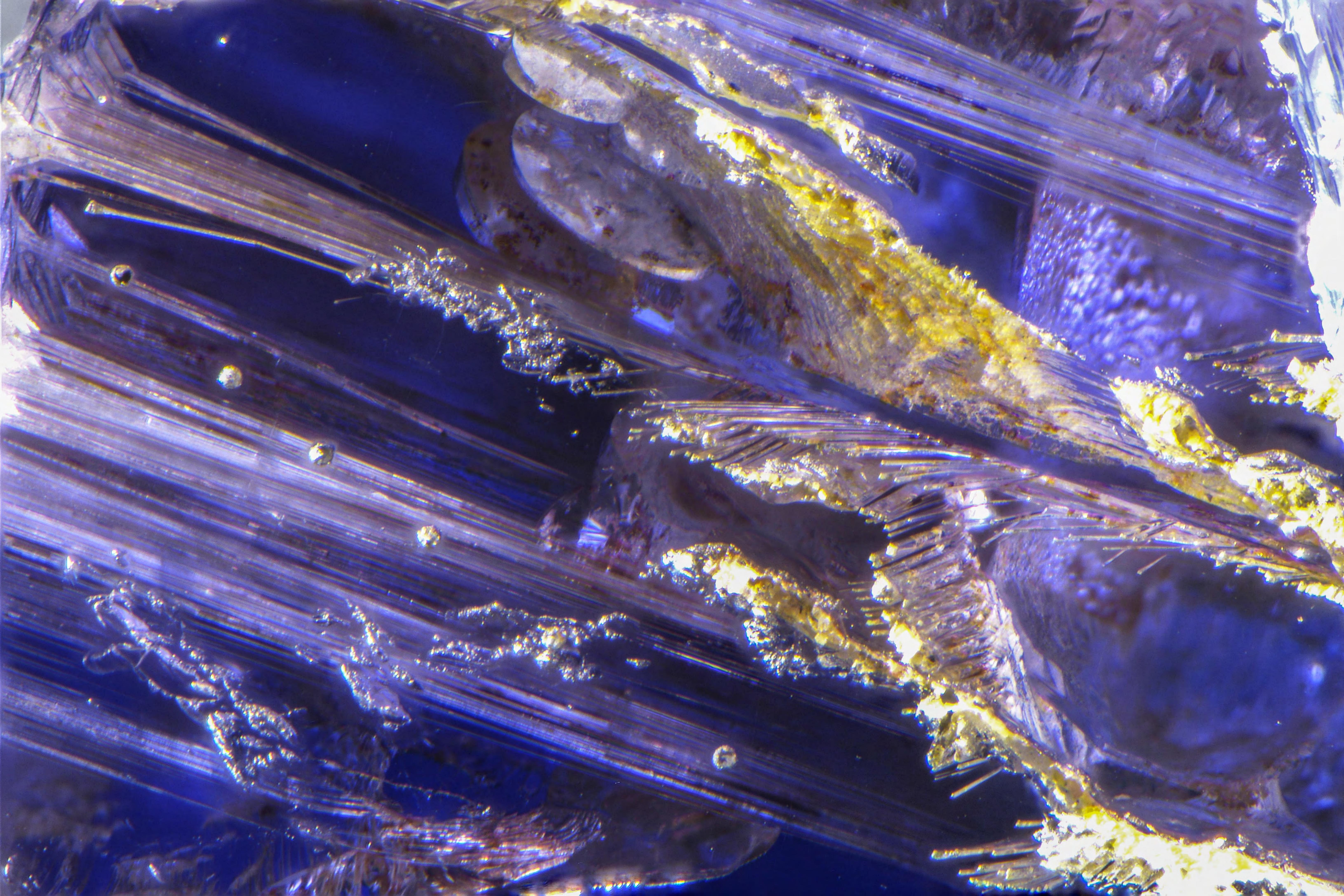


Figure 5

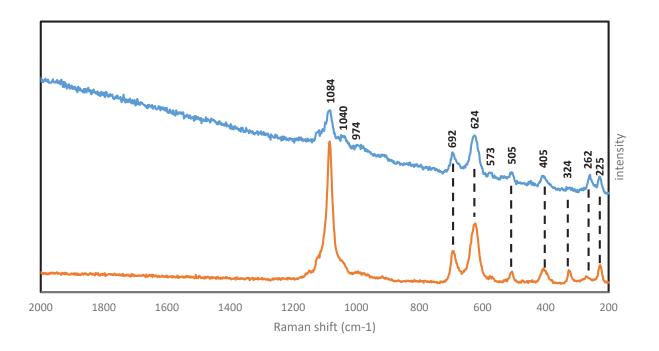


Figure 6

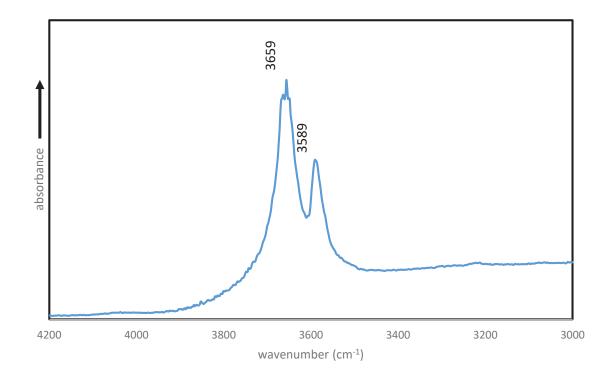


Figure 7

